Dyson orbitals for ionization from the ground and electronically excited states within equation-of-motion coupled-cluster formalism: Theory, implementation, and examples

Cite as: J. Chem. Phys. **127**, 234106 (2007); https://doi.org/10.1063/1.2805393
Submitted: 14 August 2007 . Accepted: 11 October 2007 . Published Online: 21 December 2007

C. Melania Oana, and Anna I. Krylov

Dyson orbitals for ionization from the ground and electronically excited states within equation-of-motion coupled-cluster formalism: Theory, implementation, and examples

C. Melania Oana and Anna I. Krylov[a)]
Department of Chemistry, University of Southern California, Los Angeles, California 90089-0482, USA

(Received 14 August 2007; accepted 11 October 2007; published online 21 December 2007)

Implementation of Dyson orbitals for coupled-cluster and equation-of-motion coupled-cluster wave functions with single and double substitutions is described and demonstrated by examples. Both ionizations from the ground and electronically excited states are considered. Dyson orbitals are necessary for calculating electronic factors of angular distributions of photoelectrons, Compton profiles, electron momentum spectra, etc, and can be interpreted as states of the leaving electron. Formally, Dyson orbitals represent the overlap between an initial N-electron wave function and the $N-1$ electron wave function of the corresponding ionized system. For the ground state ionization, Dyson orbitals are often similar to the corresponding Hartree-Fock molecular orbitals (MOs); however, for ionization from electronically excited states Dyson orbitals include contributions from several MOs and their shapes are more complex. The theory is applied to calculating the Dyson orbitals for ionization of formaldehyde from the ground and electronically excited states. Partial-wave analysis is employed to compute the probabilities to find the ejected electron in different angular momentum states using the freestanding and Coulomb wave representations of the ionized electron. Rydberg states are shown to yield higher angular momentum electrons, as compared to valence states of the same symmetry. Likewise, faster photoelectrons are most likely to have higher angular momentum. © *2007 American Institute of Physics*. [DOI: 10.1063/1.2805393]

I. INTRODUCTION

Photoelectron spectroscopy is a powerful technique for probing the electronic structure of molecules and ions. By measuring kinetic energy of the ejected electrons, one can determine the electronic and vibrational energy levels of the ionized system. The ensuing Franck-Condon progressions contain information on the ionization-induced structural changes from which changes in electronic wave functions can be inferred, e.g., long progressions suggest the removal of an electron from bonding or antibonding orbitals, etc. More direct probe of the initial and target electronic wave functions is possible by measuring angular distributions of the photoelectrons (PADs),[1,2] which can be recorded in essentially molecular frame by employing coincidence spectroscopy.[3] Furthermore, changes in the electronic structure in the course of a chemical reaction can be monitored by introducing time resolution in photoelectron spectroscopy.[4–7] However, retrieving the electronic structure information from the experimentally measured PADs is not a straightforward task, despite impressive progress in experimental techniques.

Different aspects of theoretical framework for calculating PADs have been developed by several groups.[8–22] Motivated by resonance enhanced multiphoton ionization (REMPI) experiments in molecular beams, the dependence of PADs on the initial and target rotational states has been worked out in meticulous details. Molecular-frame PADs appropriate for the experiments when the orientation of the system is fixed in the laboratory frame have also been discussed.[10] Recently, simulations of time-resolved PADs, which take into account nuclear dynamics, have been reported.[23–25]

A central quantity in these studies is a so-called photoelectron matrix element, which connects the initial and final wave functions,[22,26]

$$\boldsymbol{D}_{kf}^{IF} = \langle \phi_{IF}^{d}(\boldsymbol{r}) | \hat{\mu} | \Psi_{kf}^{\mathrm{el}}(\boldsymbol{r}) \rangle_{r}, \tag{1}$$

where $\hat{\mu}$ is the dipole moment operator, $\Psi_{kf}^{\mathrm{el}}(\boldsymbol{r})$ is the final (continuum) state of the ejected electron with kinetic energy determined by its momentum k, and $\phi_{IF}^{d}(\boldsymbol{r})$ is a one-electron quantity (called Dyson orbital) containing all the necessary information about N and $N-1$ electronic wave functions of the initial and the ionized states of the system,

$$\phi_{IF}^{d}(1) = \sqrt{N} \int \Psi_{I}^{N}(1, \ldots, n) \Psi_{F}^{N-1}(2, \ldots, n) d2 \ldots dn. \tag{2}$$

Dyson orbitals are also necessary for calculations of Compton profiles,[27] electron momentum spectra,[28,29] and interpretation of other orbital imaging experiments.[30–32]

For atomic ionization, the electron continuum states $\Psi_{kf}^{\mathrm{el}}(\boldsymbol{r})$ are well described by spherical waves (often referred to as partial waves), either freestanding or Coulomb, which are the exact solutions for (unbound) motion of electrons in centrally symmetric fields.[33] For molecular ionization, the potential created by the ionic core is noncentral and the partial-wave description holds only in the asymptotic limit when the electron is far from the ionized core.[18,34]

[a)]Electronic mail: krylov@usc.edu.

While considerable attention[9,18–22] has been given to calculating final states of the ionized electron, $\Psi_{kf}^{\mathrm{el}}(\boldsymbol{r})$, the molecular electronic factor $\phi_{IF}^{d}(1)$ has been treated very approximately, most often within Hartree-Fock/Koopmans framework. Effects of correlation on Dyson orbitals have been discussed,[35] mostly within Green function framework.[36]

The focus of this work is calculating Dyson orbitals from high-level *ab initio* calculations of the initial and ionized electronic wave functions by equation-of-motion coupled-cluster (EOM-CC) methods. The departure from the uncorrelated Koopmans approximation becomes particularly important when ionization of electronically excited and open-shell species is considered. The former is relevant to a wide range of experiments,[1–3,5–7] e.g., REMPI, in which n photon excitation of the initial molecule is followed by m photon ionization, or time-resolved pump-probe experiments employing ionization probe to monitor the dynamics of an electronically excited system.

It should be noted that the Dyson orbitals of Eq. (2) can be computed for any initial and target many-electron wave function, and their definition does not invoke propagator formalism.[37,38] In the latter, the Dyson orbitals are solutions of an effective one-electron equation yielding correlated ionization energies and pole strengths.[36,39,40]

The structure of the paper is as follows. The next section discusses the theoretical framework for electronic factors, Eqs. (1) and (2), their relationship to PADs, and partial-wave analysis of the outgoing electrons. Then EOM-CC methods are briefly described, and the calculation of Dyson orbitals within EOM-CC formalism is presented. The new methodology is applied to calculate Dyson orbitals for photoionization of the ground and electronically excited states of formaldehyde producing ground and excited states of the ion. The partial-wave analysis, albeit approximate, reveals interesting qualitative relationships between the character of the ionized state and the final states of the photoelectrons.

II. THEORY

A. Molecular-frame PADs and electronic wave functions

In this section, we summarize the formalism behind PADs (see Ref. 1 for an excellent review) focusing on electronic factors involved. Our presentation is done in the molecular frame and averaging over molecular orientations is discussed later.

Consider ionization of an N-electron system described by the wave function $\Psi_I^N(1,\ldots,n)$, where i denotes the spatial and spin coordinates of ith electron, $i \equiv \{x_i, y_i, z_i, \sigma_i\} = \{r_i, \theta_i, \phi_i, \sigma_i\}$, and the transformation between polar and Cartesian coordinates is given in the Appendix. Assuming that ionization is fast, i.e., within sudden ionization approximation,[8,11] the final state can be described by the independent cation and continuum wave functions, $\Psi_F^{N-1}(1,\ldots,n-1)$ and $\Psi_{kf}^{\mathrm{el}}(\boldsymbol{r},\sigma)$, respectively, with no correlation between the outgoing and the remaining $N-1$ bound electrons. The wave vector k is defined by kinetic energy of the ejected electron:

$$k = \frac{p}{\hbar} = \frac{\sqrt{2mE}}{\hbar}. \tag{3}$$

By applying time-dependent perturbation theory to describe ionization by electromagnetic field and within the dipole approximation, the probability of producing the ejected electron in the final state Ψ_{kf}^{el} is[26,33]

$$I_{IFkf} = \left| \int \Psi_I^N(1,\ldots,n)\hat{\mu}\Psi_F^{N-1}(1,\ldots,n-1) \times \Psi_{kf}^{\mathrm{el}}(n)d1\ldots dn \right|^2, \tag{4}$$

where $\hat{\mu}$ is a dipole moment operator associated with ionizing field, and all the functions and operators are expressed in the molecular frame $\boldsymbol{r}$. Invoking strong orthogonality condition, which is usually justified by vanishing overlap between the core and the ionized electron,[27,31] and by using the antisymmetric properties of the electronic wave functions and integrating over the spin coordinates, we arrive at

$$I_{IFkf} = \left| \int \phi_{IF}^{d}(\boldsymbol{r})\hat{\mu}(\boldsymbol{r})\Psi_{kf}^{\mathrm{el}}(\boldsymbol{r})d\boldsymbol{r} \right|^2 = |D_{kf}^{IF}|^2, \tag{5}$$

where $\phi_{IF}^{d}(\boldsymbol{r})$ is a Dyson orbital defined by Eq. (2) and D_{kf}^{IF} is a photoelectron matrix element from Eq. (1). Thus, the squares of the dipole matrix elements, $|D_{kf}^{IF}|^2$, give the probability to find the ionized core in state F and the ejected electron in state f for initial state I of the system.

Equation (5) may be used as a starting point for deriving PAD. The probability of finding an electron at the point $\{\theta,\phi\}$, $I_{IFkf}(\theta,\phi)$, can be obtained from Eq. (5) by changing the three-dimensional integration over $\boldsymbol{r}$ by the integration over the radial coordinate r only. Thus,

$$I_{IFkf}(\theta,\phi) = |D_{kf}^{IF}(\theta,\phi)|^2. \tag{6}$$

Alternatively, $I_{IFKf}(\theta,\phi)$ can be computed as[1]

$$I(k,\theta,\phi) = \int (\Psi_{kf}^{\mathrm{el}}(r,\theta,\phi))^{*}\Psi_{kf}^{\mathrm{el}}(r,\theta,\phi)\cdot r^2 dr. \tag{7}$$

The spatial part of the wave function of a free electron Ψ_{kf}^{el} can be expanded over the basis of spherical waves,[1]

$$\Psi_{kf}^{\mathrm{el}}(x,y,z) = \Psi_{kf}^{\mathrm{el}}(r,\theta,\phi) = \sum_{lm} C_{klm}R_{kl}(r)Y_{lm}(\theta,\phi), \tag{8}$$

where $Y_{lm}(\theta,\phi)$ are familiar spherical harmonics,

$$Y_{lm}(\theta,\phi) = \Theta_{lm}(\theta)\cdot\Phi_m(\phi) \tag{9}$$

and $R_{kl}(r)$ is a radial part, which will be discussed below. The angular and radial basis functions are orthonormal,

$$\int_0^{2\pi} \Phi_m^{*}(\phi)\Phi_m'(\phi)d\phi = \delta_{mm'}$$

$$\int_0^{\pi} Y_{lm}^{*}(\theta,\phi)Y_{l'm'}(\theta,\phi)\sin\theta d\theta d\phi = \delta_{ll'}\delta_{mm'} \tag{10}$$

$$\int_0^{\infty} r^2 R_{kl}(r)R_{k'l}(r)dr = 2\pi\delta(k'-k) = \delta(E'-E).$$

Eq. (7) then becomes

$$I(k,\theta,\phi) = \sum_{ll'mm'} C^*_{klm} C_{kl'm'} Y^*_{lm}(\theta,\phi) Y_{l'm'}(\theta,\phi) \times \int R_{kl}(r) R_{k'l'}(r) r^2 dr. \quad (11)$$

If the basis functions $R_{kl}Y_{lm}$ of expansion (8) are the eigenstates of a field-free Hamiltonian describing the ionized electron (in the potential due to the core), then the squares of the corresponding expansion coefficients $|C_{klm}|^2$ are just the squares of the following photoelectron matrix elements:

$$|C_{klm}|^2 = \left(\int \phi^{(d)}_{IF}(\mathbf{r}) \hat{\mu}(\mathbf{r}) R_{kl}(r_n) Y_{lm}(\theta,\phi) d\mathbf{r} \right)^2 \equiv |D^{IF}_{klm}|^2. \quad (12)$$

Their phases, the so-called scattering-induced phase shifts,[1] depend on the interaction of the outgoing electron with the ionized core and cannot be determined without solving some kind of a Schrödinger equation for the outgoing electron.[1] They can be defined as

$$C_{klm} = |D^{IF}_{klm}| e^{i\delta_l}. \quad (13)$$

Thus, in this case, the overall probability of Eq. (11) assumes the following simple form:

$$I(k,\theta,\phi) = \sum_{ll'mm'} |D^{IF}_{klm}| \cdot |D^{IF}_{kl'm'}| e^{i(\delta_{l'}-\delta_l)} \times \int R_{kl}(r) R_{kl'}(r) r^2 dr \cdot Y^*_{lm}(\theta,\phi) Y_{l'm'}(\theta,\phi). \quad (14)$$

This is the basis of partial-wave decomposition analysis of the final continuum states. Under the above conditions, one can easily calculate the probabilities of finding the ionized electron in a certain angular momentum state from the Dyson orbital by using Eq. (12), however, the resulting partial-wave decomposition coefficients $|D^{IF}_{klm}|$ are not sufficient for calculating the PAD, unless interference between different outgoing waves can be neglected, i.e., within random-phase approximation. This is generally not justified.[41,42]

The above assumption, i.e., that $R_{kl}Y_{lm}$ are the eigenstates of the field-free Hamiltonian describing the ionized electron, is valid only for central potentials in which exact separation of radial and angular motions is possible. This is the case of atomic ionization. The choice of R_{kl} depends on the system being ionized, e.g., for ionization of anions, the potential due to the ionized core, which is neutral, is weak and standing free waves (see the next section) are expected to be a good approximation.[34] For ionization of neutrals, a more appropriate choice of R_{kl} is the eigenfunctions of the Coulomb potential.[33] When molecular ionization is considered, two approaches are possible. Expansion (8) can be rewritten using basis functions corresponding to molecular point group symmetry,[15] as has been done for diatomics by Park and Zare.[18] Alternatively, one may still use partial waves to represent the state of the ionized electron, with the understanding that Eq. (12) and, consequently, Eq. (14) are no longer rigorously correct. Nevertheless, a small size of the core relative to the continuous final state of the electron suggests using Eqs. (12)–(14) as an approximation. This is essentially equivalent to neglecting the interaction between the core and the electron.[34] Note that even under this approximation, Eq. (12) will give rise to more partial waves in the case of molecular ionization as compared to atoms, where the selection rules are strictly $\Delta l = \pm 1$. In this work, we apply partial-wave decomposition for qualitative analysis of Dyson orbitals and selection rules of molecular ionization. We employ both the freestanding and Coulomb waves (see next section) and discuss the consequences of different choices of the radial functions.

The Dyson orbital $\phi^d(1)$ introduced by Eq. (2) is an analog of the reduced one-electron transition density matrix and can be described as an overlap between the N and $N-1$ electron wave functions of, for example, the neutral and the cation. In the second quantization form,

$$\phi^d(1) = \sum_p \gamma_p \phi_p(1), \quad (15)$$

$$\gamma_p = \langle \Psi^N | p^+ | \Psi^{N-1} \rangle, \quad (16)$$

where $\{\phi_p\}$ are the reference molecular orbitals (MOs). Dyson orbitals are not normalized, and their norms are proportional to the one-electron character of the ionization transition. For the Hartree-Fock description of the neutral, and within the Koopmans approximation for the cation, the corresponding Dyson orbitals are just the cannonical Hartree-Fock orbitals, and their norm is one. As Eqs. (5) and (12) suggest, one may interpret Dyson orbitals as wave functions of the ejected electron. For example, in a hydrogenlike atom, Dyson orbitals are just electronic wave functions of the states that are being ionized.

B. Radial functions R_{kl}

In this section we discuss two obvious choices of radial functions R_{kl} in expansion (8), i.e., the freestatnding and the Coulomb waves. In the former case, $R_{kl}(r)$ are expressed through either the half-integer or spherical Bessel functions, $J_{l+1/2}$ and j_l,[33] respectively,

$$R_{kl}(r) = \sqrt{\frac{2\pi k}{r}} J_{l+1/2}(kr) = 2k j_l(kr). \quad (17)$$

The first few members of the series are

$$R_{k0} = 2k \frac{\sin(kr)}{kr}, \quad (18)$$

$$R_{k1} = 2k \frac{\sin(kr)}{(kr)^2} - 2k \frac{\cos(kr)}{kr}, \quad (19)$$

$$R_{k2} = 6k \frac{\sin(kr)}{(kr)^3} - 2k \frac{\sin(kr)}{kr} - 6k \frac{\cos(kr)}{(kr)^2}. \quad (20)$$

The R_{kl} functions contain $\sin(kr)/(kr)^n$ and $\cos(kr)/(kr)^n$ terms and have the overall form of damped oscillations. The R_{kl} functions corresponding to kinetic energies of 0.25 and 1 eV and $l=0-5$ are plotted in Fig. 1. As one can see, the

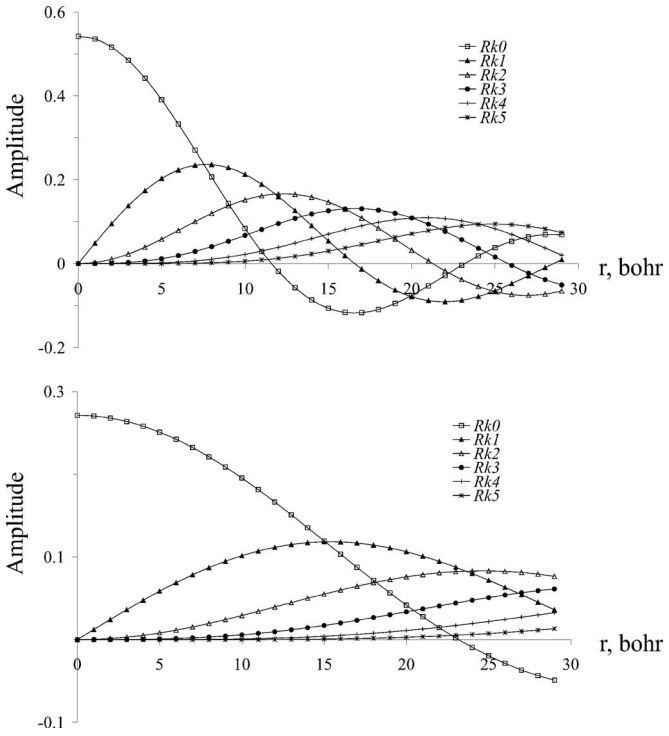

FIG. 1. Radial parts of the freestanding spherical waves, $R_{kl}(r)$ for $k=0.271$ a.u. (upper panel) and $k=0.068$ a.u. (lower panel), which correspond to photoelectron kinetic energies of 1 and 0.25 eV, respectively.

higher l is, the lower is the value of the function at small distances. Also, lower kinetic energy corresponds to longer oscillations.

It is instructive to compare R_{kl} with typical atomic orbitals, as done in Fig. 2, which displays the radial parts of the s, p, and d Gaussian-type orbitals with the exponents representative of the carbon valence shell. These orbitals extend to only about 5 Å, where only the lowest l radial functions have significant density. By virtue of Eq. (12), one can expect that ionization of Rydberg states yields higher angular momentum photoelectrons, as compared to ionization of valence states of similar symmetry. High-l states also become more probable for higher-energy electrons due to tighter oscillations in the R_{kl} functions with larger k values (i.e., Wigner law).

As kr becomes very small ($kr \ll l$), the radial functions have the following asymptotic behavior:[43]

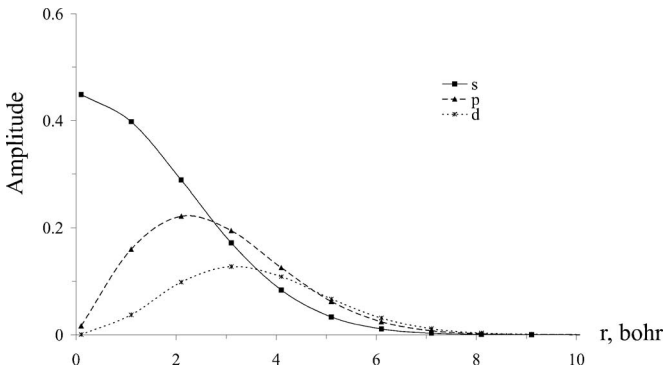

FIG. 2. Radial parts for the s, p, and d Gaussian-type orbitals with the exponent $\alpha=0.1$, a typical value for the carbon valence shell.

$$R_{kl} = 2k\frac{(kr)^l}{(2l+1)!!}. \tag{21}$$

The Coulomb waves have more complicated form that involve confluent hypergeometric functions of complex arguments.[33] In this work, we consider only the limit of very small k values ($k \to 0$), in which the radial functions can be expressed[33] through the Bessel functions,

$$R_{kl}/\sqrt{(k)}|_{k\to 0} = \sqrt{(4\pi/r)}J_{2l+1}(\sqrt{(8r)}). \tag{22}$$

The Coulomb waves for $k=0.01$ eV are plotted in Fig. 3. The most obvious difference between the Coulomb and the freestanding waves (shown in the inset) is much tighter oscillations of the former, which can be rationalized in terms of strong attractive character of the Coulomb potential. Thus, for the same Dyson orbital, the expansion in the Coulomb waves will contain higher angular momentum terms, and the dependence of the corresponding $|C_{klm}|^2$ on kinetic energy of the electrons will be less pronounced.

C. Averaging over molecular orientations

Depending on the experimental setup, different distributions of molecules are sampled by ionization, which gives rise to different types of PADs. The analytic expressions for several experimental setups have been developed using angular momentum algebra, as summarized in Ref. 1. We adopt a more flexible numerical approach that enables us to average over any spatial distribution as described below.

By introducing Euler transformations $\hat{R}_{\alpha\beta\gamma}$ and $\hat{R}^{-1}_{\alpha\beta\gamma}$ between the molecular $\{x',y',z'\}$ and the laboratory $\{x,y,z\}$ frames (see Appendix), and by considering probability $\Omega(\alpha,\beta,\gamma)$ of different molecular orientations, Eq. (12) becomes

$$\overline{|C_{klm}|^2} = \int |C_{klm}(\alpha,\beta,\gamma)|^2 \Omega(\alpha,\beta,\gamma) d\alpha d\beta d\gamma, \tag{23}$$

$$|C_{klm}(\alpha,\beta,\gamma)|^2 = \left| \int \phi^d(R_{\alpha\beta\gamma}\mathbf{r})\mu(\mathbf{r})R_{kl}(r_n)Y_{lm}(\theta_n,\phi_n)d\mathbf{r} \right|^2, \tag{24}$$

where $\overline{|C_{klm}|^2}$ are the $|C_{klm}|^2$ coefficients averaged over all molecular orientations in the laboratory frame. If all molecular orientations are equally probable, i.e., $\Omega(\alpha,\beta,\gamma)=1/4\pi$, most of the information about the Dyson orbital is lost. To avoid the loss of information, the molecules could be prealigned prior to ionization event, e.g., by electronic excitation or by selecting a particular rotational state. Finally, in coincidence experiments,[3,44] the photoelectrons can be recorded in the recoil frame, thus allowing one to retrieve the information about the Dyson orbital essentially in the molecular frame. Below we discuss averaging for two common experimental setups.

Let us consider photoionization from electronically excited states, when the molecules are selected by the first laser (assume the first laser is polarized along z axis). The prob-

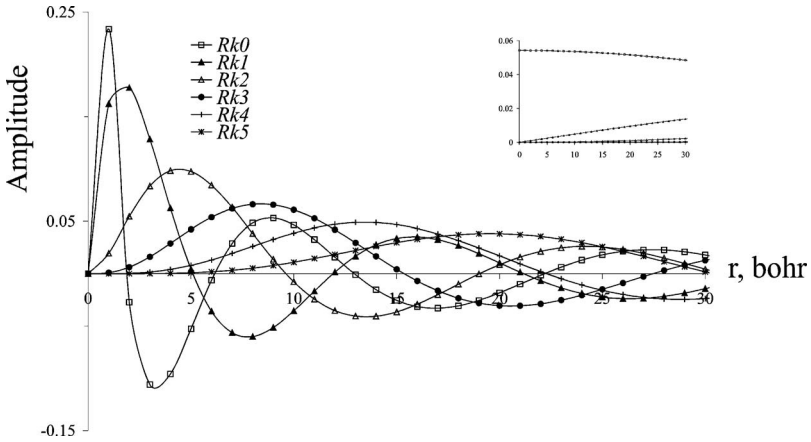

FIG. 3. Radial parts of the Coulomb waves, $R_{kl}(r)$ for $k=0.002\,71$ a.u. ($E_k=0.01$ eV). Inset: The corresponding freestanding spherical waves in the same r range.

ability of a molecule to be excited is proportional to the scalar product between the laser dipole $\boldsymbol{\mu}_l=z$ and the dipole moment of an electronic transition $\boldsymbol{\mu}_{\mathrm{el}}$,

$$\Omega(\alpha,\beta,\gamma)=(R^{-1}_{\alpha\beta\gamma}\mu_{\mathrm{el}}\cdot z)^2. \tag{25}$$

For diatomic molecules, the above yields two simple expressions, for the parallel and perpendicular electronic transitions,

$$\Omega^{\mathrm{par}}(\alpha,\beta,\gamma)=\cos^2(\beta), \tag{26}$$

$$\Omega^{\mathrm{per}}(\alpha,\beta,\gamma)=\sin^2(\beta). \tag{27}$$

In coincidence experiments, if molecules are aligned along z axis, only averaging over the azimuthal angle α should be conducted, as well as averaging between parallel and antiparallel (with respect to z axis) orientations.

D. Ionized, electron-attached, and electronically excited states within EOM-CCSD formalism

Conceptually, EOM approach[45–52] is similar to configuration interaction (CI): Target EOM states are found by diagonalizing the so-called similarity transformed Hamiltonian $\bar{H}\equiv e^{-T}He^{T}$,

$$\bar{H}R=ER, \tag{28}$$

$$L\bar{H}=LE, \tag{29}$$

$$LR=1, \tag{30}$$

where T, R, and L^+ are general excitation operators with respect to the reference determinant $|\Phi_0\rangle$. Due to the non-Hermitian nature of $\bar{H}$, its left eigenstates L are not Hermitian conjugates of R. Regardless of the choice of T, the spectrum of $\bar{H}$ is exactly the same as that of the original Hamiltonian H—thus, in the limit of the complete many-electron basis set, EOM is identical to full configuration interaction. In a more practical case of a truncated basis, e.g., when T and R are truncated at single and double excitations, the EOM models are numerically superior to the corresponding CI models,[53] because correlation effects are "folded in" in the transformed Hamiltonian. Moreover, the truncated EOM models are size consistent (or, more rigorously, size intensive), provided that the amplitudes T satisfy the CC equations for the reference state $|\Phi_0\rangle$,

$$\langle\Phi_\mu|\bar{H}-E|\Phi_0\rangle=0, \tag{31}$$

where Φ_μ denotes μ-tuply excited determinants, e.g., $\{\Phi_i^a,\Phi_{ij}^{ab}\}$ in the case of coupled-cluster singles and doubles (CCSD).

By combining different types of excitation operators and references $|\Phi_0\rangle$, different groups of target states can be accessed, as explained, for example, in Refs. 52 and 54. In the ionized/electron-attached EOM models,[55–58] operators R are not electron conserving (i.e., include different numbers of creation and annihilation operators),

$$\Psi^{N-1}=R^{\mathrm{IP}}\Psi^N_{\mathrm{CCSD}}=R^{\mathrm{IP}}e^{T_1+T_2}\Phi_0,$$
$$R^{\mathrm{IP}}=\sum_i r_i i+\frac{1}{2}\sum_{ija} r^a_{ij}a^+ji, \tag{32}$$

where Ψ^N_{CCSD} and Φ_0 are the reference CCSD wave functions and the reference Slater determinant of the neutral, respectively. Thus, for the ionization from the electronic ground state, Dyson orbitals are defined as

$$\gamma^R_p=\langle\Phi_0e^{-(T_1+T_2)}(1+\Lambda)|p^+|R^{\mathrm{IP}}e^{T_1+T_2}\Phi_0\rangle,$$
$$\gamma^L_p=\langle\Phi_0e^{-(T_1+T_2)}L^{\mathrm{IP}}|p|e^{T_1+T_2}\Phi_0\rangle. \tag{33}$$

Electronically excited states can be described when the reference $|\Phi_0\rangle$ corresponds to the ground state wave function, and operators R conserve the number of electrons and the total spin,[47,49,59]

$$\Psi^N_{\mathrm{ex}}=R^{\mathrm{EE}}\Psi^N_{\mathrm{CCSD}}=R^{\mathrm{EE}}e^{T_1+T_2}\Phi_0, \tag{34}$$

$$R^{\mathrm{EE}}=r_0+\sum_{ia} r^a_i a^+i+\frac{1}{4}\sum_{ijab} r^{ab}_{ij}a^+b^+ji, \tag{35}$$

and the corresponding Dyson orbitals are thus

$$\gamma^R_p=\langle\Phi_0e^{-(T_1+T_2)}L^{\mathrm{EE}}|p^+|R^{\mathrm{IP}}e^{T_1+T_2}\Phi_0\rangle,$$
$$\gamma^R_p=\langle\Phi_0e^{-(T_1+T_2)}L^{\mathrm{IP}}|p^+|R^{\mathrm{EE}}e^{T_1+T_2}\Phi_0\rangle, \tag{36}$$

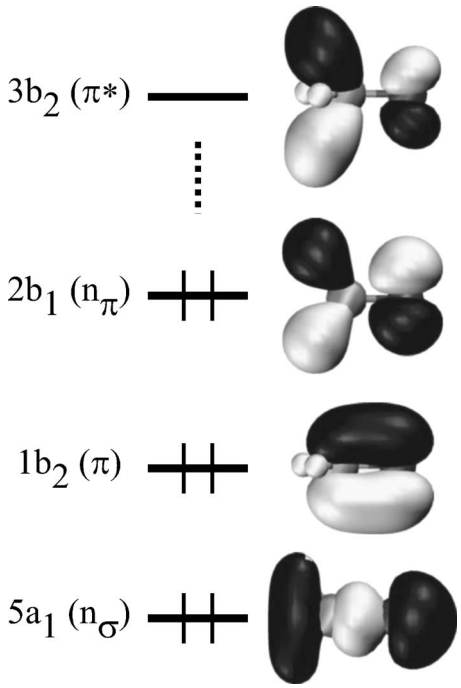

FIG. 4. Relevant MOs of formaldehyde.

Similarly to one-particle transition density matrices in EOM-CC for excitation energies (EOM-EE) theory,[49] the "right" and "left" Dyson orbitals, γ_p^R and γ_p^L, are not identical, and Eq. (12) should be rewritten as

$$|C_{klm}|^2 = \int \phi^{d,R}(\mathbf{r})\mu(\mathbf{r})R_{kl}(r_n)Y_{lm}(\theta_n,\phi_n)d\mathbf{r} \cdot \int \phi^{d,L}(\mathbf{r})\mu(\mathbf{r})R_{kl}(r_n)Y_{lm}^*(\theta_n,\phi_n)d\mathbf{r}. \quad (37)$$

Since the same reference CCSD wave function is employed in both EOM-IP and EOM-EE calculations, the evaluation of Dyson orbitals is very straightforward and does not require to deal with nonorthogonal MO sets.

We implemented Dyson orbitals for the CCSD/EOM-EE-CCSD/EOM-SF-CCSD and EOM-IP/EA-CCSD wave functions of the initial and ionized/electron-attached states, respectively. EOM-EE-CCSD includes single ($1h1p$, 1-hole-1-particle) and double ($2h2p$) excitations in the EOM part, see Eq. (35), and is therefore appropriate for electronically excited states that are dominated by single-electron excitations. The SF variant allows us to consider initial states of a diradical or triradical character, as well as some doubly excited states.[54] EOM-IP-CCSD, which includes $1h$ and $2h1p$ operators in the EOM part, see Eq. (32), is capable of describing states dominated by Koopmans-type ($1h$) excitations including the states with several singly ionized configurations strongly mixed in the target wave function. EOM-EA-CCSD includes $1p$ and $1h2p$ operators and allows access to other types of open-shell states.

Our implementation of Dyson orbitals within EOM uses a simple modification of our general EOM-CCSD code[51] following the elegant idea first employed by Stanton who pointed out that simply by adding a very diffuse orbital (e.g., the size of Earth) to the basis and generating guess vectors that include excitations to/from this orbital is equivalent to ionization/attachment. Thus, Dyson orbitals are simply the corresponding row/column in the EOM-EE transition density matrices.[51,60] Their norms are proportional to the one-electron character of the ionizing excitation. The two-electron character of the ionization can be estimated only from the two-particle transition density matrices,

$$\gamma_{pqs}^R = \langle \Phi_0 e^{-(T_1+T_2)} L^{\mathrm{EE}} | p^+ q^+ s | R^{\mathrm{IP}} e^{T_1+T_2} \Phi_0 \rangle, \quad (38)$$

$$\gamma_{pqs}^L = \langle \Phi_0 e^{-(T_1+T_2)} L^{\mathrm{IP}} | s^+ qp | R^{\mathrm{EE}} e^{T_1+T_2} \Phi_0 \rangle. \quad (39)$$

For ionization transitions that have mainly two-electron character, the Dyson orbital norm is close to zero.

TABLE I. Vertical ionization energies (eV) and leading contributions to Dyson orbitals for the ionization of CH_2O in its ground state producing various states of the cation, EOM-IP-CCSD/6-311G(2+,2+)G**.

CH_2O^+ state	IE (eV)	Dyson orbital
$X\ ^2B_1$ $(n_\sigma^2\pi^2n_\pi^1)$	10.63	98.7% ϕ_{2b_1}
$1\ ^2B_2$ $(n_\sigma^2\pi^1n_\pi^2)$	14.35	99.8% ϕ_{1b_2}
$1\ ^2A_1$ $(n_\sigma^1\pi^2n_\pi^2)$	15.90	99.1% ϕ_{5a_1}

E. Implementation details

Our implementation consists of the two major parts: (i) Calculation of Dyson orbitals, and (ii) the partial-wave decomposition analysis and averaging. The first part, which is based on Eqs. (16), (33), and (36), requires calculation of correlated wave functions of the initial and target states and is implemented within the EOM-CC suite of codes in the Q-CHEM electronic structure package.[61] The Dyson orbitals are expressed in terms of the reference MOs, see Eq. (16), and the normalized coefficients γ_p, as well as the norms of the orbitals, are printed in the output. The values of the Dyson orbital on a cubic grid can also be computed and plotted using visualization software, e.g., VMD.[62]

The second part, which is a separate computer program, calculates $|C_{klm}|^2$, see Eq. (24), for specified k values and up to a maximum l and specified polarization of ionizing radiation. The calculations are performed either in the molecular frame, or, if averaging over the molecular orientations is requested, over the $\{\alpha_i,\beta_j,\gamma_k\}$ grid with subsequent averaging, Eq. (23). The evaluation of integral [Eq. (24)] is done numerically on the cubic $\{\mathbf{r}_{lmn}=(x_l,y_m,z_n)\}$ grid in the laboratory frame as follows. At each grid point $\mathbf{r}_{lmn}$, the values of

TABLE II. Vertical excitation energies for selected valence (V) and Rydberg (R) excited states of formaldehyde, calculated at the EOM-CCSD/6-311(2+,2+)G** level of theory (Ref. 68).

State	E_{ex} (eV)
$5\ ^1A_1$ (V)	10.00
$1\ ^1A_2$ (V)	3.94
$2\ ^1A_2$ (R)	8.22
$3\ ^1A_2$ (R)	9.63
$1\ ^1B_1$ (R)	7.05
$1\ ^1B_2$ (V)	9.25
$2\ ^1B_2$ (R)	10.75

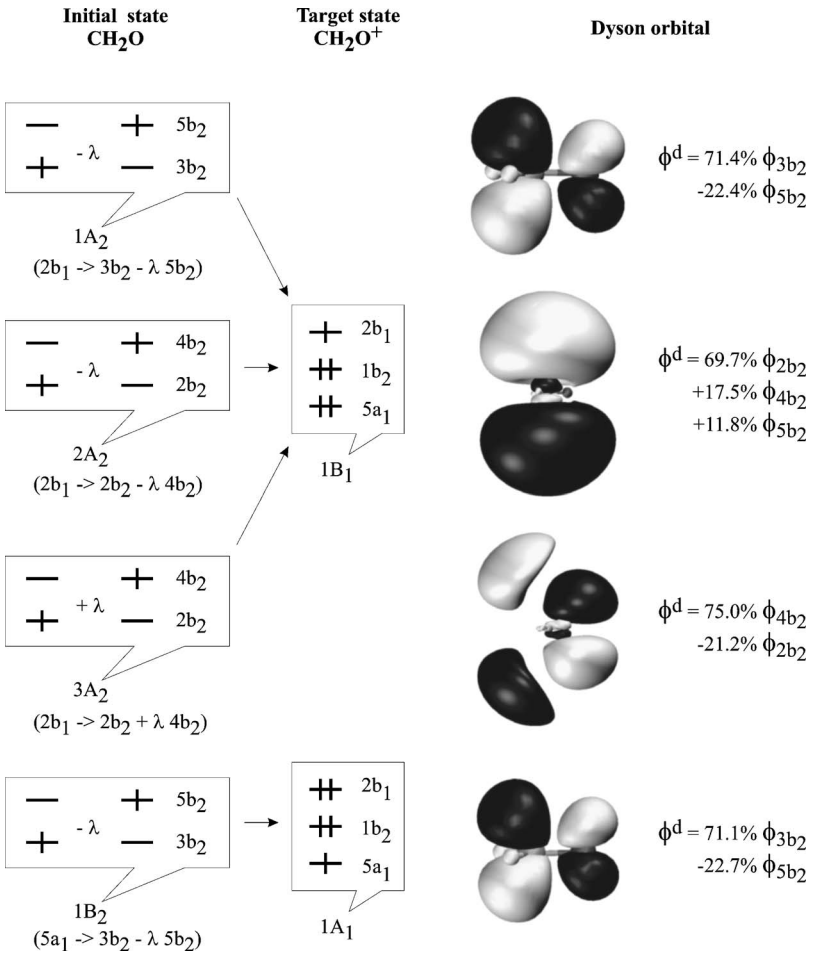

FIG. 5. Dyson orbitals for the $^1A_2$ and 1 $^1B_2$ excited state ionizations of formaldehyde. The leading electronic configurations are shown for each state. Only the excited electron MOs are shown for each state; the rest of the electrons occupy the same MOs as in the corresponding state of the cation.

spherical waves are calculated using analytical expressions (see below), and the value of the Dyson orbital in the laboratory frame is computed by making the transformation to the molecular frame, Eq. (A4), and calculating $\phi^d(R_{\alpha\beta\gamma}\mathbf{r})$ from the MO coefficients and analytic expressions of the atomic basis functions.

The position of $R_{kl}Y_{lm}$ and, consequently, the decomposition coefficients $|C_{klm}|^2$ depend on the origin of the laboratory coordinate system, which is unabigously defined only in the spherically symmetric systems. For molecular systems, we chose the center of density of the (left) Dyson orbital as the origin of the laboratory and molecular frames,

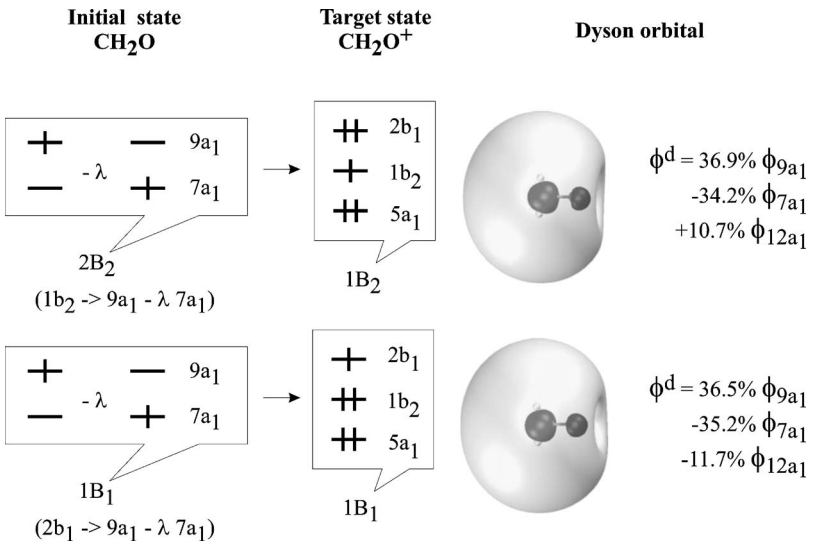

FIG. 6. Dyson orbitals for the 1 $^1B_1$ and 2 $^1B_2$ excited state ionizations of formaldehyde. The leading electronic configurations are shown for each state. Only the excited electron MOs are shown for each state; the rest of the electrons occupy the same MOs as in the corresponding state of the cation.

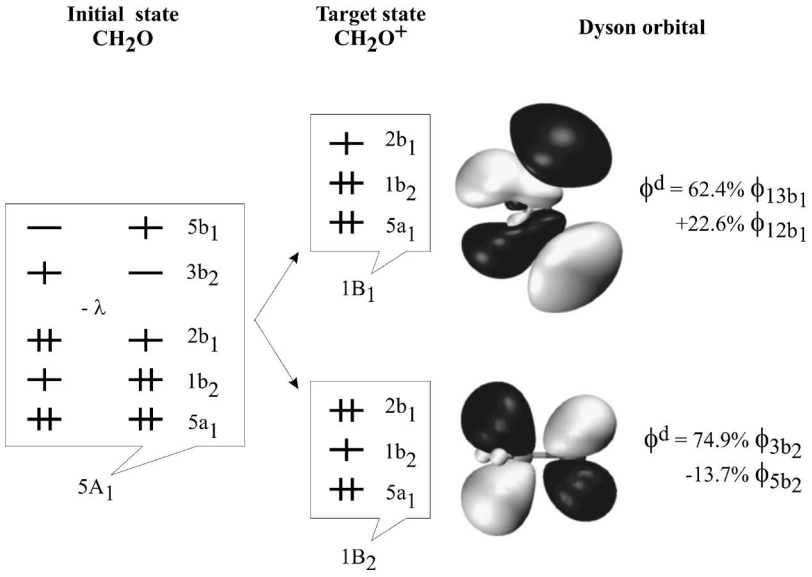

FIG. 7. Dyson orbitals for the $5\ ^1A_1$ excited state ionizations of formaldehyde.

$$\bar{x} = \int \phi^d(r) x \phi^d(r) dxdydz,$$

$$\bar{y} = \int \phi^d(r) y \phi^d(r) dxdydz, \tag{40}$$

$$\bar{z} = \int \phi^d(r) z \phi^d(r) dxdydz.$$

In the case of atomic systems, the above $\{\bar{x},\bar{y},\bar{z}\}$ correspond to the atom position. This choice is equivalent to orthogonality condition of the state of ionized electron to the Dyson orbital from the pont of view of Eq. (1).

The Bessel functions that enter the spherical waves expression, Eq. (17), are implemented in the GNU SCIENTIFIC LIBRARY.[63] Alternatively, they can be easily calculated using recurrence relations.[43] At the small intramolecular r distances used to calculate Dyson orbitals, often $kr \ll l$, and the asymptotic formula in Eq. (21) should be used. Our numeric tests show that there is no general threshold value $(kr/l)_{\min}$ for using Eq. (21). For $l=3-11$, the kr/l threshold decreases almost linearly as l increases, and one could fit a function $f(l)=al+b$ for the calculation of $(kr/l)_{\min}$. However, for precision the exact threshold for each l was used in our calculations. The Coulomb waves are also implemented in the GNU SCIENTIFIC LIBRARY,[63] with the $l>kr$ restriction, which does not always hold for our applications, especially when $l=0$. Thus, we restricted our implementation of the Coulomb waves to very small k values, as in Eq. (22). The final $|\overline{C_{klm}}|^2$ values are stored in a binary file, for subsequent PAD modeling, which gives a flexibility of calculating PADs in different representations.

III. FORMALDEHYDE EXAMPLE

In this section we present the results for ionization of formaldehyde from its ground and electronically excited states of different characters. Our goal is to develop qualitative understanding of the relation between the electron configurations of the neutral molecule and its cation and the shape of the corresponding Dyson orbital. We consider ionizing transitions of the following three types: (i) Same initial state producing different final states; (ii) same final states obtained from different initial states; (iii) different initial and final states. We calculate the probabilities of different l, m angular momentum states of the photoionized electron and rationalize the results by extending the atomic selection rules to delocalized MOs using Eq. (12). Detailed data on the computed Dyson orbitals are given in EPAPS.[64] Correlated Dyson orbitals for inner and outer valence ionizations of the ground-state formaldehyde have been reported and employed to interpret electron momentum and Compton profiles.[65–67]

A. Dyson orbitals

The frontier MOs of formaldehyde are depicted in Fig. 4. The highest occupied orbitals have n_σ, π, and n_π bonding characters, while lowest unoccupied molecular orbital is the π^* MO. Removing an electron from highest occupied molecular orbital (HOMO) $(n_\pi, 2b_1)$ leads to the ground state

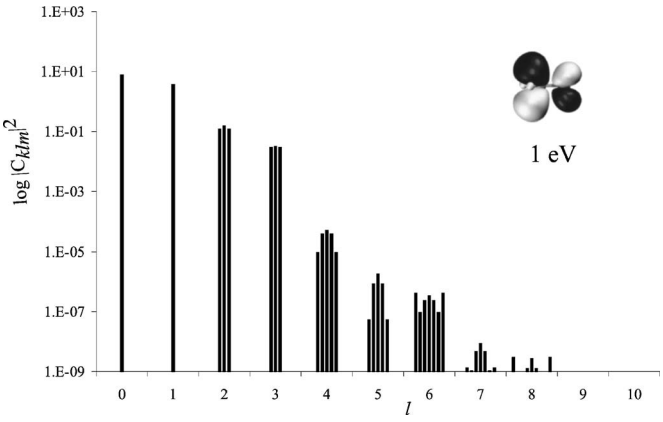

FIG. 8. Probabilities of finding photoelectrons in different l, m states for ionization of the $1\ ^1A_2$ excited state of formaldehyde producing the $1\ ^2B_1$ ground state. The corresponding Dyson orbital is also shown. Ionization polarization is along the y axis. Bars clustered around an l value correspond to different $m=-1\cdots l$ values.

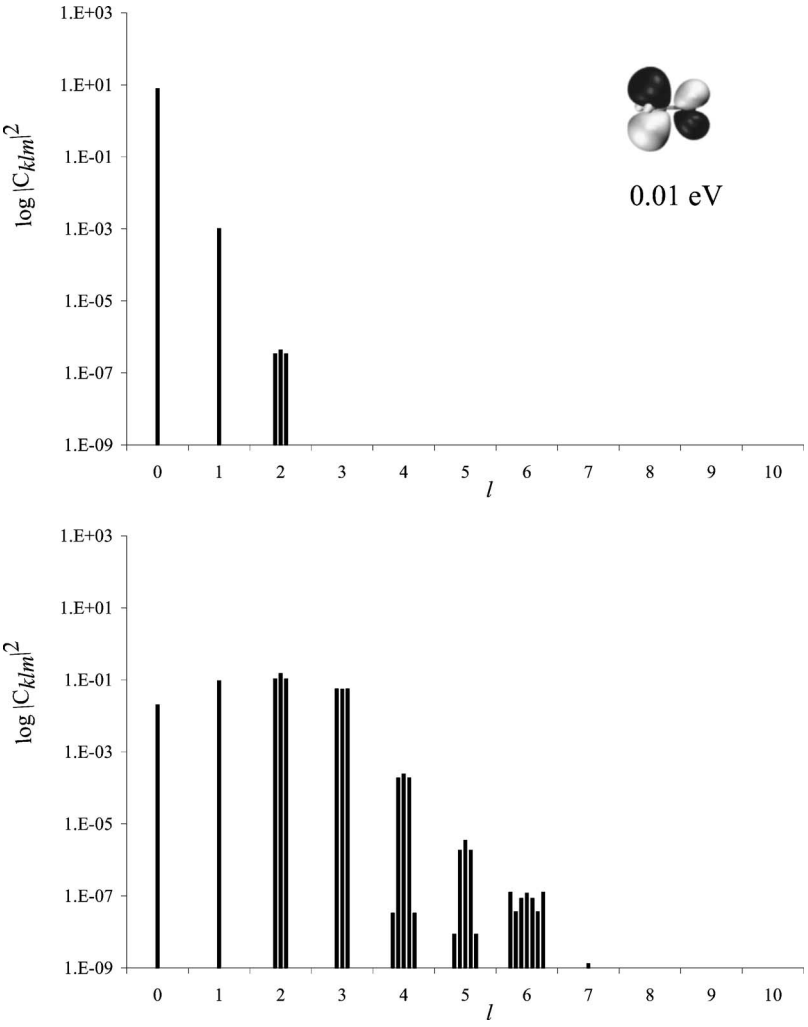

FIG. 9. Probabilities of obtaining different l, m states of photoelectrons for ionization of the $1\,^1A_2$ excited state of formaldehyde producing the $1\,^2B_1$ ground state, in the limit of small kinetic energy (0.01 eV), calculated using the freestanding (upper panel) and the Coulomb (lower panel) spherical waves. The corresponding Dyson orbital is also shown. Ionization polarization is along the y axis. Bars clustered around an l value correspond to different $m=-l\cdots l$ values.

$(X\,^2B_1)$ of the CH_2O^+ cation, while ionizations of the lower MOs give rise to the $1\,^2B_2$ and $1\,^2A_1$ excited states (see Table I).

For Hartree-Fock (HF) wave functions and within the Koopmans approximation, the Dyson orbitals for each of the above ground state ionizations are just the corresponding canonical MOs of CH_2O. When correlation is taken into account at the CCSD and EOM-IP-CCSD levels of theory [using the 6-311(2+,2+)G^{*+} basis], the Dyson orbitals remain essentially unchanged and retain almost 100% Koopmans character, as summarized in the last column of Table I, which contains leading contributions to the corresponding Dyson orbitals in terms of the canonical Hartree-Fock MOs. This is not surprising for a well-behaved, closed-shell molecule whose ground-state wave function is dominated by a single electronic configuration and the cation states are nondegenerate. However, for ionization from excited states, in which multiple configurations are present, we expect significant differences with respect to the Koopmans picture.

The electronically excited states of formaldehyde are summarized in Table II. The lowest valence singlet excited state $1\,^1A_2$ corresponds to the $n_\pi \rightarrow \pi^*$ excitation. From about 7 eV onward, several valence and Rydberg excited states appear.[68] We consider only one-electron transitions, for which the norm of Dyson orbitals is relatively large.

The wave function of the lowest valence excited state $1\,^1A_2$ contains two major configurations, corresponding to the $2b_1(n_\pi)\rightarrow 3b_2(\pi^*)$ and $2b_1\rightarrow 5b_2$ (Rydberg) excitations. The lowest state of the cation, which can be derived from one-electron ionization of this excited state, is the $1\,^2B_1$ ground state. The calculated Dyson orbital is shown in Fig. 5 and consists of the $3b_2$ MO (71.4%), $5b_2$ (92.4%), as well as smaller contributions from other b_2 MOs. This composition reflects the relative weights of Slater determinants that form the initial $1\,^1A_2$ excited state (64.0% and 21.1%, respectively), as calculated from the EOM-EE amplitudes.

The next valence excited state is $1\,^1B_2$, which corresponds to excitations to the same pair of MOs ($3b_2$ and $5b_2$), but from the lower $5a_1(n_\sigma)$ orbital. Ionization leads to the $1\,^2B_2$ excited state of CH_2O^+. The Dyson orbital MO composition for this $1\,^1B_2\rightarrow 1\,^2A_1$ transition is almost the same as for the above $1\,^1A_2\rightarrow 1\,^2B_1$ ionization, despite different characters of the initial and final states. What the two transitions have in common is the "wave function" of the leaving electron: In both cases it is a combination of the $3b_2$ and $5b_2$ MOs. These Dyson orbitals are also similar to the $3b_2$ MO because $3b_2$ and $5b_2$ MOs have approximately the same angular distribution and differ only by their radial dependence. For one-electron ionizations, Dyson orbitals can be estimated semiquantitatively by considering the ionization of each of the electronic configurations of the initial state wave function, without relaxing the remaining occupied orbitals. Thus,

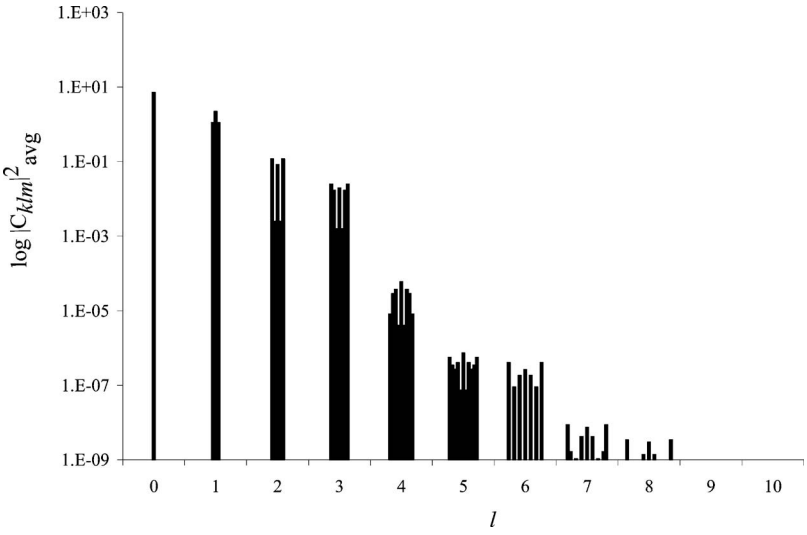

FIG. 10. Probabilities of finding photoelectrons in different l, m states for ionization of the $1\ ^1A_2$ excited state of formaldehyde producing the $1\ ^2B_1$ ground state. Ionization laser is polarized along the y axis, perpendicular to the molecular plane, and cylindrical averaging around the y axis is conducted. Bars clustered around an l value correspond to different $m=-l\cdots l$ values.

a Koopmans-type picture applies to the ionization of multiconfigurational wave functions, which provides useful guidelines for rationalizing the shapes of complicated Dyson orbitals for excited state ionization.

The Koopmans-type picture also emerges from considering ionization of Rydberg excited states. The $X\ ^1B_1$ and $2\ ^1B_2$ states consist mainly of excitations to the $9a_1$ and $7a_1$ Rydberg MOs from the $2b_1(n_\pi)$ and $1b_2(\pi)$ orbitals, respectively, as shown in Fig. 6. The Dyson orbitals for these $1\ ^1B_1 \rightarrow X\ ^2B_1$ and $2\ ^1B_2 \rightarrow 1\ ^2B_2$ ionization transition contain approximately the same combination of a_1 MOs due to the similarity of the excited electron wave functions.

Let us now analyze the Dyson orbitals for the transitions between the *different* excited states of the neutral and the *same* target state of the cation. The first three $^1A_2$ states of formaldehyde represent excitations from the HOMO to different b_2 MOs; the resulting cation is in the ground $1\ ^2B_1$ state. The $1\ ^1A_2$ state corresponds to excitations to the already discussed $3b_2$ and $5b_2$ MOs, while the next two states are the excitations to the *plus* and, respectively, *minus* combinations of $2b_2$ and $4b_2$ Rydberg MOs. As seen from Fig. 5, the shapes of the Dyson orbitals for these $n\ ^1A_2 \rightarrow 1\ ^2B_1 (n=1-3)$ ionizations are very different indeed. This is easily rationalized because the orbital levels of the leaving electron are not the same: $3b_2-5b_2$, $2b_2+4b_2$, $2b_2-4b_2$. For the last two Dyson orbitals, the $2b_2:4b_2$ ratio is directly related to the relative weights of the corresponding amplitudes in the $2\ ^1A_2$ and $3\ ^1A_2$ wave functions: 63.7% $2b_2+16.2\%$ $4b_2$, and, respectively, 69.1% $2b_2-19.5\%$ $4b_2$.

The norms of Dyson orbitals, as discussed in Sec. II, are related to one-electron character of the transition. In the case of formaldehyde, the norm of all Dyson orbitals for one electron ionizations is found to be about 0.12. Our calculations of other small molecules show that the norm of Dyson orbitals for one-electron ionization is approximately constant for a given molecular species. An interesting case is the $5\ ^1A_1$ excited state of formaldehyde (Fig. 7), which involves two different types of excitations: $1b_2(\pi) \rightarrow 3b_2(\pi^*)$ and $2b_1(n_\pi) \rightarrow 5b_1$ (Rydberg). Thus, ionization could lead to either the $1\ ^2B_2$ or $X\ ^2B_1$ cation states. The norms of the

TABLE III. The largest $|C_{klm}|^2$ coefficients ($>10^{-4}$) for three formaldehyde ionization transitions: (A) $1\ ^1A_2(V) \rightarrow X\ ^2B_1$, molecular frame, (B) $1\ ^1A_2(V) \rightarrow 1\ ^2B_1$, averaging around y, (C) $2\ ^1A_2(R) \rightarrow 1\ ^2B_1$, molecular frame. Ionization polarization is along the y axis, perpendicular to the molecular plane, and $k=0.271$ a.u. ($E_k=1$ eV).

		$\lvert C_{klm}\rvert^2$		
l	$\lvert m\rvert$	A	B	C
0	0	7.8	7.1	5.3×10^{1}
1	0	3.7	2.2	2.0×10^{-3}
	1	...[a]	1.1	...
2	0	1.6×10^{-1}	8.3×10^{-2}	1.2×10^{2}
	1	...	2.5×10^{-3}	...
	2	1.2×10^{-1}	1.2×10^{-1}	1.8×10^{2}
3	0	3.1×10^{-2}	1.9×10^{-2}	3.8×10^{-2}
	1	...	1.6×10^{-3}	...
	2	2.9×10^{-2}	1.7×10^{-2}	2.3×10^{-2}
	3	...	2.5×10^{-2}	...
4	0			6.8×10^{-2}
	1			...
	2	$10^{-5}-10^{-6}$[b]	$10^{-5}-10^{-6}$	4.1×10^{-2}
	3			...
	4			7.7×10^{-2}
5	0			
	1			
	2	$10^{-6}-10^{-8}$	$10^{-7}-10^{-8}$	$10^{-5}-10^{-7}$
	3			
	4			
	5			
6	0			2.2×10^{-3}
	1			...
	2			1.6×10^{-3}
	3	$10^{-7}-10^{-8}$	$10^{-7}-10^{-8}$	...
	4			8.4×10^{-4}
	5			...
	6			3.3×10^{-3}

[a]Zero coefficients, due to symmetry.
[b]For $|C_{klm}|^2<10^{-4}$, only the order of magnitude of the highest coefficients is given.

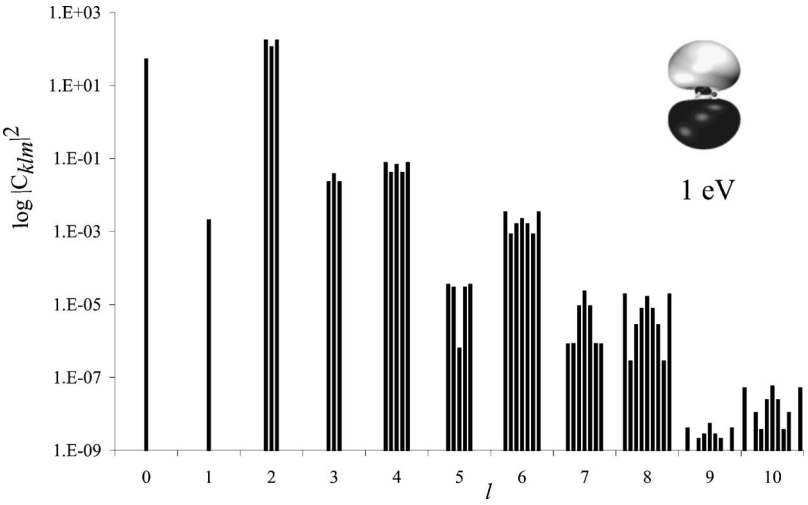

FIG. 11. Probabilities of finding photoelectrons in different l, m states for ionization of the $2\ ^1A_2$ excited state of formaldehyde producing the $1\ ^2B_1$ ground state. The corresponding Dyson orbital is also shown. Ionization polarization is along the y axis. Bars clustered around an l value correspond to different $m=-l\cdots l$ values.

$5\ ^1A_1 \rightarrow X\ ^2B_2$ and $5\ ^1A_1 \rightarrow X\ ^2B_1$ Dyson orbitals are 0.078 and, respectively, 0.042, the sum of the values being 0.12.

B. Partial-wave decomposition: The $|C_{klm}|^2$ coefficients

The squares of the C_{klm} coefficients give the probability of obtaining a photoelectron with l, m angular momentum, and wave number k, under the assumption that $R_{kl}Y_{lm}$ are eigenstates of the ejected electrons (see Sec. II A). For ionization of atoms the allowed states are $\Delta l=\pm 1$ with respect to the Dyson orbital l quantum number. In the molecular case, Dyson orbitals have lower symmetry, and the selection rules are less strict.

Depending on the experimental setup, averaging over molecular orientations is often necessary, see Eq. (23). To demonstrate the effect of the averaging on the C_{klm}, we consider azimuthal averaging around the y molecular axis, which would correspond to an experiment where the molecules are oriented perpendicular to the laser ionization polarization. Cylindrical averaging is conducted, for example, in Stolow's experiments on the NO dimer,[44,69] which motivated the present work. We also calculated the $|C_{klm}|^2$ coefficients for non-averaged CH_2O Dyson orbitals, in order to understand qualitatively the major l, m contributions.

Consider again ionization of formaldehyde from its lowest valence excited state to the ground state cation, $1\ ^1A_2 \rightarrow 1\ ^2B_1$ (Fig. 5). Figure 8 shows the probabilities of producing different l, m angular momentum states. The highest coefficients are obtained for $l=0$, 1, 2, and 3. This is consistent with the shape of the orbital: This b_2 Dyson orbital could be decomposed approximately into d and p_y orbitals. By extension of the atomic selection rules, the allowed Y_{lm} states would be indeed s, d, and p, f. The coefficients for other l states are several orders of magnitude lower, although they are not zero as would be in the atomic case. Thus, by decomposing the delocalized Dyson orbitals into different same-center orbital contributions, one can rationalize the l, m angular momentum states of the photoelectron. However, this is possible only when Dyson orbitals have relatively simple shapes.

It is interesting to compare the $|C_{klm}|^2$ coefficients obtained using the freestanding and Coulomb wave representations of the photoelectron wave function. The l, m decomposition for the two cases, in the limit of very small k (0.01 eV) are shown in Fig. 9. For the free-standing spherical waves, there is a large difference among the s, p, and d contributions due to the low density of the $l>0$ waves in the small r Dyson orbital region. For the Coulomb waves, the l, m expansion extends to higher angular momentum and the $l=0-2$ coefficients are within one order of magnitude. Thus, one can expect that ionization of neutral species will produce higher angular momentum photoelectrons than that of anions, assuming similar shapes of the corresponding Dyson orbitals.

After cylindrical averaging around the y axis, one obtains the average coefficients $|C_{klm}|^2$ in Fig. 10, using spherical wave representation. The highest coefficients correspond to the $l=0-3$ angular momentum, but more m states become populated. By rotating the molecular frame, the x,y,z projections of the electron angular momentum in the laboratory frame change.

The highest $|C_{klm}|^2$ contributions (above 10^{-4}) are given in Table III. Note that even the coefficients that give the major contributions differ by a few orders of magnitude. This is due to the smaller overlap of R_{kl} radial functions with high l at smaller intramolecular distances (see Sec. II B). Therefore, high angular momentum states of the electron become more accessible for ionization of the Rydberg states. For comparison, Fig. 11 displays the $|C_{klm}|^2$ decomposition of the b_2 Dyson orbital corresponding to the $2\ ^1A_2 \rightarrow X\ ^2B_1$ ionization. The angular distribution of this Dyson orbital is similar to the previous one, but the increase in number of radial nodes and the higher density at large radius result in larger contributions from high l states, especially 4 and 6. Finally, Fig. 12 compares the $|C_{klm}|^2$ values computed using the free-standing and the Coulomb waves for this Dyson orbital. The resulting trend, higher angular momentum states for the Coulomb waves, is similar to that observed for the valence $1\ ^1A_2 \rightarrow X\ ^2B_1$ ionization.

The data shown in Figs. 8–12 are given in the EPAPS supplement.[64]

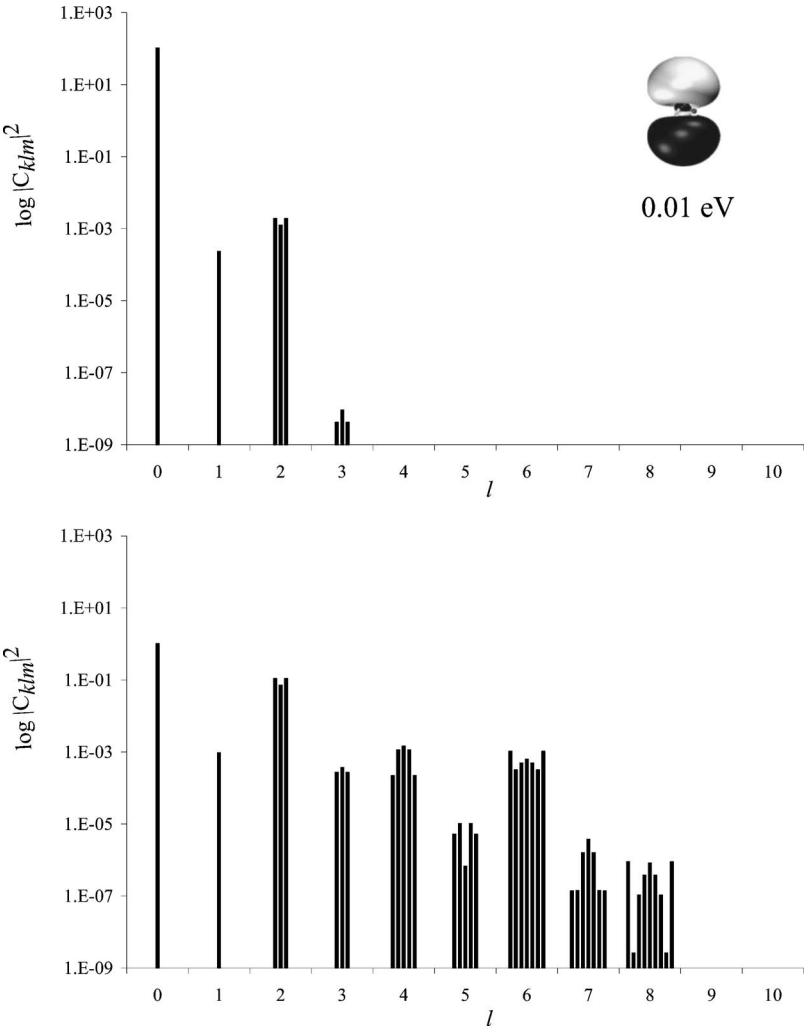

FIG. 12. Probabilities of finding photoelectrons in different l, m states for ionization of the $2\ ^1A_2$ excited state of formaldehyde producing the $1\ ^2B_1$ ground state, calculated using the freestanding (upper panel) and the Coulomb (lower panel) spherical waves, in the limit of small kinetic energy (0.01 eV). The corresponding Dyson orbital is also shown. Ionization polarization is along the y axis. Bars clustered around an l value correspond to different $m=-l\cdots l$ values.

IV. CONCLUSIONS

We report the implementation of Dyson orbitals within the EOM-CC family of methods. Formally, Dyson orbitals represent the overlap between an N-electron wave function of the molecule and the $N-1/N+1$ electron wave function of the corresponding cation/anion, and are required for calculating PADs, Compton profiles, electron momentum spectra, and are relevant for other orbital imaging experiments. In the case of ionizing transitions, they can be interpreted as states of the leaving electron and are required for calculating electronic factors of angular distributions of photoelectrons. Correlated Dyson orbitals are especially important for ionization of electronically excited and open-shell species. As demonstrated by the formaldehyde example, Dyson orbitals of the ground-state closed-shell molecules are well approximated by the corresponding HF molecular orbitals. For ionization of species with multiconfigurational wave functions, the shapes of the Dyson orbitals are more complex, however, they still can be rationalized within Koopmans-type picture, i.e., by considering leading EOM amplitudes in the Hartree-Fock MO representation.

A complete PAD modeling requires the wave function of the ionized electron to account for interference effects and core-electron interactions, and will be pursued in a future work. Under certain approximations, however, the Dyson orbitals can be employed in partial-wave decomposition, that is, for evaluating the probabilities of finding the ionized electron in different angular momentum states. We discuss partial-wave analysis and apply it to formaldehyde. The wave function of the ionized electron is approximated by an expansion in partial waves, either freestanding or Coulomb. For relatively simple molecular Dyson orbitals, the $|C_{klm}|^2$ contributions can be rationalized by decomposition of the Dyson MO into different l, m same-center orbitals and the extension of the atomic selection rules. Due to low density of spherical waves at small r, ionization of Rydberg states is more likely to produce higher angular momentum electrons. Likewise, faster electrons are more likely to have higher angular momentum. Anion ionization leading to neutral species should favor lower angular momentum electrons due to the longer oscillations of the freestanding versus the Coulomb spherical waves. Thus, although quantitative simulation of PADs involves more sophisticated treatment, simple partial-wave decomposition of Dyson orbitals reveals interesting trends that can be applied to the qualitative interpretation of experimental PADs.

ACKNOWLEDGMENTS

Support from the National Science Foundation (Grant No. CHE-0616271) is gratefully acknowledged. C.M.O. is

Wise Postdoctoral Fellow and acknowledges support from the Wise Research Fund (USC). We thank Professor Hanna Reisler and Professor David Yarkony for stimulating discussions and insightful comments. This work is conducted under auspices of the *iOpenShell* Center for Computational Studies of Electronic Structure and Spectroscopy of Open-Shell and Electronically Excited Species supported by the National Science Foundation through the CRIF:CRF CHE-0625419 +0624602+0625237 grant.

APPENDIX: TRANSFORMATION BETWEEN POLAR AND CARTESIAN COORDINATES

Transformation from polar to Cartesian coordinates is given by

$$x = r\cos(\phi)\sin(\theta), \tag{A1}$$

$$y = r\sin(\phi)\sin(\theta), \tag{A2}$$

$$z = r\cos(\theta). \tag{A3}$$

An arbitrary rotation of a rigid body can be described by the three sequential transformations, i.e., Euler rotations,[70]

$$\boldsymbol{r}' = R_{\alpha\beta\gamma}\boldsymbol{r} = R_z(\alpha)R_y(\beta)R_z(\gamma)\boldsymbol{r}, \tag{A4}$$

where $\boldsymbol{r}$ denotes the coordinates in a fixed laboratory frame and $\mathbf{r}'$—in a molecular frame rotating with the body. Operators $R_{x_i}(\phi)$ describe rotation by angle ϕ around laboratory axis x_i and assume the following simple form:

$$R_z(\alpha) = \begin{pmatrix} \cos(\alpha) & -\sin(\alpha) & 0 \\ -\sin(\alpha) & \cos(\alpha) & 0 \\ 0 & 0 & 1 \end{pmatrix}, \tag{A5}$$

$$R_y(\beta) = \begin{pmatrix} \sin(\beta) & \cos(\beta) & 0 \\ 0 & 0 & 1 \\ \cos(\beta) & -\sin(\beta) & 0 \end{pmatrix}. \tag{A6}$$

The inverse transformation from the molecular to the laboratory-fixed frame is readily obtained as

$$R^{-1}_{\alpha\beta\gamma} = R_z^{-1}(\gamma)R_y^{-1}(\beta)R_z^{-1}(\alpha) = R_z(-\gamma)R_y(-\beta)R_z(-\alpha). \tag{A7}$$

The ranges for α, β, and γ are $0\ldots 2\pi$, $0\ldots\pi$ and $0\ldots 2\pi$, respectively.

The orientation of a diatomic molecule is uniquely defined by one angle describing the orientation of molecular axis with respect to, for example, z axis, and the corresponding Euler transformation is thus $R_y(\beta)$. For nonlinear molecules in coincidence experiments, when one of the molecular axes is fixed, e.g., as in $(NO)_2$ with the *NN* axis coinciding with the laboratory axis z, there remains only one degree of freedom, rotation around z axis, $R_z(\alpha)$.

[1] K. L. Reid, Annu. Rev. Phys. Chem. **54**, 397 (2003).
[2] K. Wang and V. McKoy, Annu. Rev. Phys. Chem. **46**, 275 (1995).
[3] R. E. Continetti, Annu. Rev. Phys. Chem. **52**, 165 (2001).
[4] M. Seel and W. Domcke, J. Chem. Phys. **95**, 7806 (1991).
[5] D. M. Neumark, Annu. Rev. Phys. Chem. **52**, 255 (2001).
[6] T. Seideman, Annu. Rev. Phys. Chem. **53**, 41 (2002).
[7] A. Stolow, Annu. Rev. Phys. Chem. **54**, 89 (2003).
[8] B. T. Pickup and O. Goscinsky, Mol. Phys. **26**, 1013 (1973).
[9] D. Dill and J. L. Dehmer, J. Chem. Phys. **61**, 692 (1974).
[10] D. Dill, J. Chem. Phys. **65**, 1130 (1976).
[11] B. T. Pickup, Chem. Phys. **19**, 193 (1977).
[12] Y. Itikawa, Chem. Phys. **28**, 461 (1978).
[13] S. N. Dixit and V. McKoy, J. Chem. Phys. **82**, 3546 (1985).
[14] N. Chandra, Chem. Phys. **108**, 301 (1986).
[15] N. Chandra, J. Phys. B **20**, 3405 (1987).
[16] K. L. Reid, D. J. Leahy, and R. N. Zare, J. Chem. Phys. **95**, 1746 (1991).
[17] D. J. Leahy, K. L. Reid, and R. N. Zare, J. Chem. Phys. **95**, 1757 (1991).
[18] H. Park and R. N. Zare, J. Chem. Phys. **104**, 4554 (1996).
[19] R. R. Lucchese, G. Raseev, and V. McKoy, Phys. Rev. A **25**, 2572 (1982).
[20] I. Powis, Chem. Phys. **201**, 189 (1995).
[21] N. A. Cherepkov, S. K. Semenov, Y. Hikosaka, K. Ito, and A. Yaghisita, Phys. Rev. Lett. **84**, 250 (2000).
[22] I. Cacelli, R. Moccia, and A. Rizzo, Phys. Rev. A **57**, 1895 (1998).
[23] Y. Arasaki, K. Takatsuka, K. Wang, and V. McKoy, J. Chem. Phys. **112**, 8871 (2000).
[24] M. T. do N. Varella, Y. Arasaki, H. Ushiyama, V. McKoy, and K. Takatsuka, J. Chem. Phys. **124**, 154302 (2006).
[25] H. R. Hudock, B. G. Levine, A. L. Thompson, H. Satzger, D. Townsend, N. Gador, S. Ulrich, A. Stolow, and T. J. Martínez, J. Phys. Chem. A **111**, 8500 (2007).
[26] H. A. Bethe and E. E. Salpeter, *Quantum Mechanics of One and Two Electron Atoms* (Plenum, New York, 1977).
[27] I. G. Kaplan, B. Barbiellini, and A. Bansil, Phys. Rev. B **68**, 235104 (2003).
[28] E. Weigold and I. E. McCarthy, *Electron Momentum Spectroscopy* (Kluwer, Dordecht/Plenum, New York, 1999).
[29] M. S. Deleuze and S. Klippenberg, J. Chem. Phys. **125**, 104309 (2006).
[30] J. Itatani, J. Levesque, D. Zeidler, H. Niikura, H. Pépin, J. C. Kieffer, P. B. Corkum, and D. M. Villenueve, Nature (London) **432**, 867 (2004).
[31] S. Patchkovskii, Z. Zhao, T. Brabec, and D. M. Villenueve, Phys. Rev. Lett. **97**, 123003 (2006).
[32] M. Yamazaki, T. Horio, N. Kishimoto, and K. Ohno, Phys. Rev. A **75**, 032721 (2007).
[33] L. D. Landau and E. M. Lifshitz, *Quantum Mechanics: Non-Relativistic Theory* (Pergamon, Oxford, 1977).
[34] D. Hanstrop, C. Bengtsson, and D. J. Larson, Phys. Rev. A **40**, 670 (1987).
[35] L. S. Cederbaum, W. Domcke, J. Schrimer, and W. Von Niessen, Adv. Chem. Phys. **65**, 115 (1986).
[36] L. S. Cederbaum and W. Domcke, Adv. Chem. Phys. **36**, 205 (1977).
[37] A. A. Abrikosov, L. P. Gorkov, and J. E. Dzyaloskinski, *Methods of Quntum Field Theory in Statistical Physics* (Prentice-Hall, Englewood Cliffs, NJ, 1963).
[38] A. L. Fetter and J. D. Walecka, *Quantum Theory of Many Particle Systems* (McGraw-Hill, New York, 1971).
[39] J. Linderberg and Y. Öhrn, *Propagators in Quantum Chemistry* (Academic, London, 1973).
[40] J. V. Ortiz, Adv. Quantum Chem. **35**, 33 (1999).
[41] J. Cooper and R. N. Zare, J. Chem. Phys. **48**, 942 (1968).
[42] J. L. Hall and M. W. Siegel, J. Chem. Phys. **48**, 943 (1968).
[43] G. B. Arfken, *Mathematical Methods for Physicists* (Elsevier Academic, Burlington, MA, 2005).
[44] O. Gessner, A. M. D. Lee, J. P. Shaffer, H. Reisler, S. Levchenko, A. Krylov, J. G. Underwood, H. Shi, A. L. L. East, D. M. Wardlaw, E. t-H. Chrysostom, C. C. Hayden, and A. Stolow, Science **311**, 219 (2006).
[45] D. J. Rowe, Rev. Mod. Phys. **40**, 153 (1968).
[46] K. Emrich, Nucl. Phys. A **351**, 379 (1981).
[47] H. Sekino and R. J. Bartlett, Int. J. Quantum Chem., Quantum Chem. Symp. **18**, 255 (1984).
[48] J. Geertsen, M. Rittby, and R. J. Bartlett, Chem. Phys. Lett. **164**, 57 (1989).
[49] J. F. Stanton and R. J. Bartlett, J. Chem. Phys. **98**, 7029 (1993).
[50] R. J. Bartlett and J. F. Stanton, Rev. Comput. Chem. **5**, 65 (1994).
[51] S. V. Levchenko and A. I. Krylov, J. Chem. Phys. **120**, 175 (2004).
[52] A. I. Krylov, Annu. Rev. Phys. Chem. **59**, 433 (2008).
[53] J. Olsen, J. Chem. Phys. **113**, 7140 (2000).
[54] A. I. Krylov, Acc. Chem. Res. **39**, 83 (2006).
[55] D. Sinha, D. Mukhopagedhyay, and D. Mukherjee, Chem. Phys. Lett. **129**, 369 (1986).
[56] S. Pal, M. Rittby, R. J. Bartlett, D. Sinha, and D. Mukherjee, Chem.

Phys. Lett. **137**, 273 (1987).
[57] J. F. Stanton and J. Gauss, J. Chem. Phys. **101**, 8938 (1994).
[58] M. Nooijen and R. J. Bartlett, J. Chem. Phys. **102**, 3629 (1995).
[59] H. Koch, H. J. Aa. Jensen, P. Jørgensen, and T. Helgaker, J. Chem. Phys. **93**, 3345 (1990).
[60] S. V. Levchenko, T. Wang, and A. I. Krylov, J. Chem. Phys. **122**, 224106 (2005).
[61] Y. Shao, L. F. Molnar, Y. Jung, J. Kussmann, C. Ochsenfeld, S. Brown, A. T. B. Gilbert, L. V. Slipchenko, S. V. Levchenko, D. P. O'Neil, R. A. Distasio, Jr., R. C. Lochan, T. Wang, G. J. O. Beran, N. A. Besley, J. M. Herbert, C. Y. Lin, T. Van Voorhis, S. H. Chien, A. Sodt, R. P. Steele, V. A. Rassolov, P. Maslen, P. P. Korambath, R. D. Adamson, B. Austin, J. Baker, E. F. C. Bird, H. Daschel, R. J. Doerksen, A. Drew, B. D. Dunietz, A. D. Dutoi, T. R. Furlani, S. R. Gwaltney, A. Heyden, S. Hirata, C.-P. Hsu, G. S. Kedziora, R. Z. Khalliulin, P. Klunziger, A. M. Lee, W. Z. Liang, I. Lotan, N. Nair, B. Peters, E. I. Proynov, P. A. Pieniazek, Y. M. Rhee, J. Ritchie, E. Rosta, C. D. Sherrill, A. C. Simmonett, J. E. Subotnik, H. L. Woodcock III, W. Zhang, A. T. Bell, A. K. Chakraborty, D. M. Chipman, F. J. Keil, A. Warshel, W. J. Herhe, H. F. Schaefer III, J. Kong, A. I. Krylov, P. M. W. Gill, and M. Head-Gordon, Phys. Chem. Chem. Phys. **8**, 3172 (2006).
[62] W. Humphrey, A. Dalke, and K. Schulten, J. Mol. Graphics **14**, 33 (1996).
[63] http://www.gnu.org/software/gsl/
[64] See EPAPS Document No. E-JCPSA6-127-303744 for the molecular geometry, Dyson orbital coefficients, and partial-wave decomposition data. This document can be reached through a direct link in the online article's HTML reference section or via the EPAPS homepage (http://www.aip.org/pubservs/epaps.html).
[65] A. O. Bawagan, C. E. Brion, E. R. Davidson, C. Boyle, and R. F. Frey, Chem. Phys. **128**, 439 (1988).
[66] M. Roux and I. R. Epstein, Chem. Phys. Lett. **18**, 18 (1973).
[67] S. R. Langhoff and R. A. Tawil, J. Chem. Phys. **63**, 2745 (1975).
[68] A. I. Krylov, C. D. Sherrill, and M. Head-Gordon, J. Chem. Phys. **113**, 6509 (2000).
[69] S. Levchenko, H. Reisler, A. Krylov, O. Gessner, A. Stolow, H. Shi, and A. L. L. East, J. Chem. Phys. **125**, 084301 (2006).
[70] J. J. Sakurai, *Modern Quantum MEchanics* (Addison-Wesley, Reading, MA, 1995).
[71] M. Head-Gordon, R. J. Rico, M. Oumi, and T. J. Lee, Chem. Phys. Lett. **219**, 21 (1994).